# Decreasing the coordinated N atoms in a single-atom Cu catalyst to achieve selective transfer hydrogenation of alkynes†

Xuge Zhang,‡[ab] He Lin,‡[c] Jian Zhang,‡*[b] Yajun Qiu,[a] Zedong Zhang,[a] Qi Xu,[a] Ge Meng,[b] Wensheng Yan, [ID][d] Lin Gu, [ID][e] Lirong Zheng, [ID][f] Dingsheng Wang [ID]*[a] and Yadong Li [ID][a]

Single-atom (SA) catalysts have attracted broad attention due to their distinctive catalytic properties in diverse reactions. Increasing the unsaturated coordination sites of active centers is a valid and challenging approach to improve the performance of such catalysts. Herein, we report an oxide compounding strategy to decrease the N coordination number of a SA Cu catalyst by reducing the thickness of the N-doped carbon carrier with a lower density of N atoms. The SA Cu catalyst with a more unsaturated N coordination structure can achieve transfer hydrogenation of alkynes with good activity and selectivity, which is disabled over the common N coordinated SA Cu catalyst on pure CN. It is found that individual Cu centers coordinated by fewer N atoms can accelerate the hydrogen transfer from ammonia–borane and still leave proper adsorption sites for alkynes to realize the entire hydrogenation reaction. This work will open up new opportunities to modulate the unsaturated coordination structure of SA catalysts for creating better-performing heterogeneous catalysts.

## Introduction

Single-atom (SA) catalysts have recently attracted much attention[1–4] due to their unique performance in numerous fields such as electrochemistry,[5–8] organic synthesis[9–12] and industrial catalysis.[13–15] The specific properties of such catalysts derive from the low coordination of metal centers, which affords a peculiar electronic structure and favorable adsorption of reactants.[16–18] For now, SA catalysts on N-doped carbon (CN) have emerged as versatile and classic catalysts, and are usually obtained from the pyrolysis of organic polymers[19,20] or metal–organic frameworks.[21,22] It is noteworthy that the general metal

centers in such catalysts inevitably suffer from saturated coordination by abundant N atoms in pure CN due to the better stability, which restricts their catalytic behavior in many cases.[23,24] Thus, an effective strategy to regulate the coordination environment of metal centers for increasing unsaturated sites is crucial to enhance their catalytic performance.[25–27] So far, a limited number of approaches have been reported to tailor the coordination number of metal centers in CN supported SA catalysts like changing pyrolysis temperature,[28,29] choosing different precursors[30,31] and altering the immobilization of metal.[32–34] Therefore, it is urgent but tough to develop new pathways to modulate the unsaturated coordination structures of SA catalysts on CN and further disclose their impact on the catalytic activity.

Semihydrogenation of alkynes represents the most convenient and straightforward method to produce olefins, the important intermediates[35–37] and raw chemical material[38–40] in organic synthesis. Benefitting from the superior reusability, a few heterogeneous catalysts have been applied in this transformation.[41–45] However, these heterogeneous catalysts are mainly based on a noble metal with selectivity issues or suffering from harsh reaction conditions (high temperature and high pressure of H₂). Thus, it is highly desirable to develop more abundant non-noble metal based heterogeneous catalysts for such reaction with good selectivity under mild conditions. For this purpose, heterogeneous base metal catalyzed transfer hydrogenation of alkynes provides a potential approach for avoiding the high pressure of H₂.[46,47] In this context, active

*ªDepartment of Chemistry, Tsinghua University, Beijing 100084, China. E-mail: wangdingsheng@mail.tsinghua.edu.cn*

*ᵇCollege of Chemistry and Materials Engineering, Wenzhou University, Wenzhou, Zhejiang 325035, China. E-mail: zhangjian@wzu.edu.cn*

*ᶜState Key Laboratory of Chemistry and Utilization of Carbon Based Energy Resources, Key Laboratory of Advanced Functional Materials, Autonomous Region, Institute of Applied Chemistry, College of Chemistry, Xinjiang University, Urumqi, 830046, Xinjiang, China*

*ᵈNational Synchrotron Radiation Laboratory, CAS Center for Excellence in Nanoscience, University of Science and Technology of China, Hefei 230029, China*

*ᵉBeijing National Laboratory for Condensed Matter Physics, Institute of Physics, Chinese Academy of Sciences, Beijing 100190, China*

*ᶠBeijing Synchrotron Radiation Facility, Institute of High Energy Physics, Chinese Academy of Sciences, Beijing 100049, China*

† Electronic supplementary information (ESI) available. See DOI: 10.1039/d1sc04344g

‡ These authors contributed equally to this work.

metal centers need to serve as the station to transfer hydrogen species from the hydrogen source to alkynes, which demands enough adsorption sites for the hydrogen source and alkynes.[48] Thus, it is essential to fabricate targeted base metal heterogeneous catalysts with more unsaturated coordination sites.

Herein, we demonstrate an oxide compounding CN strategy to reduce coordinated N atoms in a SA Cu catalyst for realizing transfer semihydrogenation of alkynes. Owing to the CN on an $Al_2O_3$ matrix being thinner with decreased doped N atoms, the general $Cu–N_3$ and $Cu–N_4$ features of a SA Cu catalyst on pure CN can be tuned to the more unsaturated $Cu–N_2$ feature. The obtained $Cu–N_2$ structure makes the SA Cu catalyst succeed in achieving transfer hydrogenation of alkynes, which cannot occur over $Cu–N_3$ and $Cu–N_4$ structures. The optimized SA Cu catalyst exhibits good activity and selectivity to produce a variety of olefins. It is clarified that the lower-coordination state of the $Cu–N_2$ structure benefits hydrogen species transferring from ammonia–borane (AB) to Cu centers, and simultaneously affords the appropriate adsorption site for alkynes to complete the hydrogenation reaction smoothly.

## Results and discussion

The SA Cu catalyst supported on pure CN (denoted as $Cu_1$/CN) is prepared through pyrolyzing melamine–formaldehyde (MF) resin with loading of Cu (Fig. S1†).[49] To increase the unsaturated coordination sites of the SA Cu catalyst, the MF resin loaded Cu is generated on an $Al_2O_3$ matrix *via* the *in situ* polymerization process followed by the same pyrolysis treatment

(denoted as $Cu_1$/CN/$Al_2O_3$) (Fig. S1†). The irregular thick nanosheet morphology of $Cu_1$/CN can be observed in high-resolution transmission electron microscopy (HR-TEM) and scanning transmission electron microscopy (STEM) images (Fig. 1a and S2†). Meanwhile, for $Cu_1$/CN/$Al_2O_3$, a thin CN coating layer can be distinguished from the $Al_2O_3$ matrix (Fig. 1b), which is formed from the coated MF resin as revealed by HR-TEM and Fourier transform infrared (FT-IR) analyses (Fig. S3 and S4†). No visible Cu or its derivative nanoparticles can be found in either of the two catalysts by HR-TEM, STEM or X-ray diffraction (XRD) analysis (Fig. 1a and b, S2, S5 and S6†). The homogeneous distribution of Cu and N species on the two catalysts is confirmed through energy dispersive X-ray (EDX) elemental mapping experiments (Fig. 1c and d). The presence of SA Cu species is verified by aberration corrected high-angle annular dark-field scanning transmission electron microscopy (AC HAADF-STEM) measurements which show a number of bright dots assigned to independent Cu species on $Cu_1$/CN and $Cu_1$/CN/$Al_2O_3$ (Fig. 1e and f). The loading content of Cu is determined to be 1.65 and 0.98 wt% for $Cu_1$/CN and $Cu_1$/CN/$Al_2O_3$ according to inductively coupled plasma optical emission spectrometry (ICP-OES) tests.

The local atomic and electronic structures of the two catalysts are investigated by X-ray absorption spectroscopy (XAS) techniques. As shown in Fourier transformed extended X-ray absorption fine structure (FT-EXAFS) spectra at the Cu K-edge (Fig. 2a, for EXAFS in *k*-space see Fig. S7†), there is only one primary peak attributed to the Cu–N bond (~1.5 Å) but no other peaks of the Cu–Cu bond (~2.1 Å) are observed for $Cu_1$/CN or
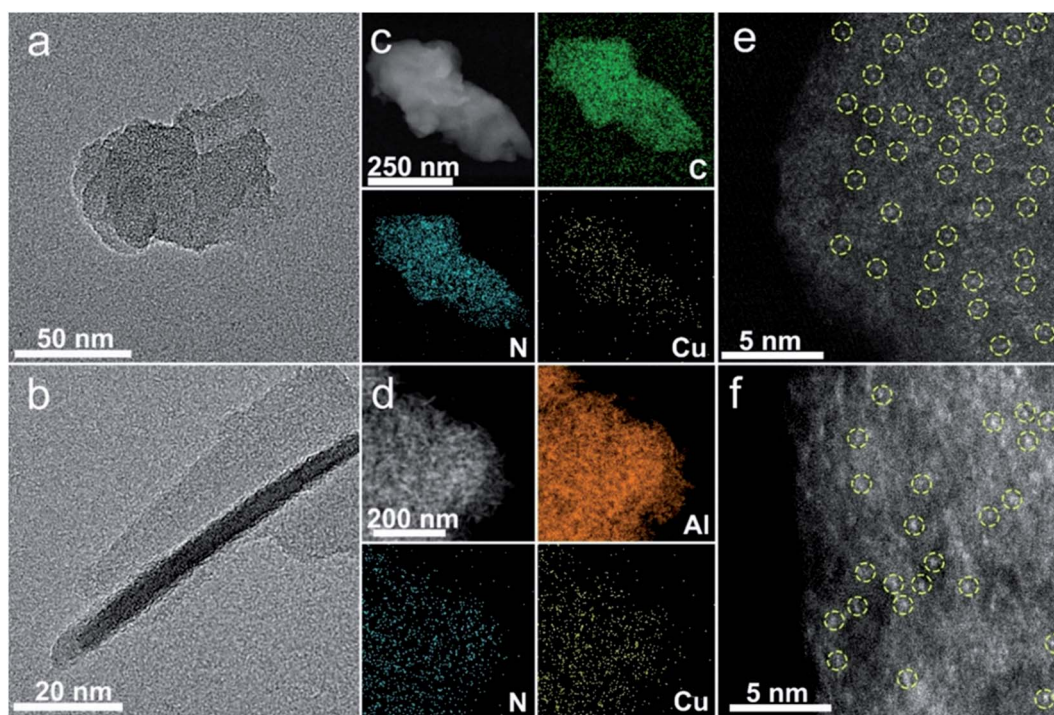


**Fig. 1** Characterization of $Cu_1$/CN and $Cu_1$/CN/$Al_2O_3$. (a) HR-TEM image of $Cu_1$/CN. (b) HR-TEM image of $Cu_1$/CN/$Al_2O_3$. (c) EDX elemental mapping analysis of $Cu_1$/CN. (d) EDX elemental mapping analysis of $Cu_1$/CN/$Al_2O_3$. (e) Representative AC HAADF-STEM image of $Cu_1$/CN. (f) Representative AC HAADF-STEM image of $Cu_1$/CN/$Al_2O_3$. The yellow circles in e and f are drawn around partial SA Cu species.
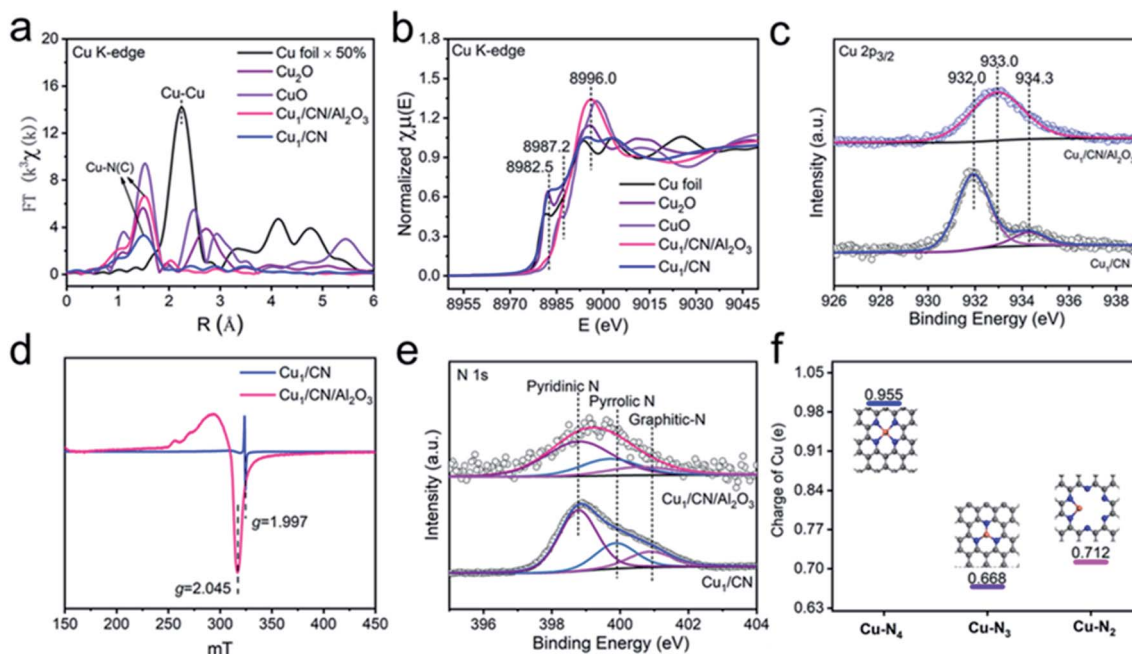
**Fig. 2** Structural analyses of $Cu_1/CN$ and $Cu_1/CN/Al_2O_3$. (a) FT-EXAFS spectra of $Cu_1/CN$ and $Cu_1/CN/Al_2O_3$ with CuO, $Cu_2O$ and Cu foil as references at the Cu K-edge. (b) XANES spectra of $Cu_1/CN$ and $Cu_1/CN/Al_2O_3$ with CuO, $Cu_2O$ and Cu foil as references at the Cu K-edge. (c) Deconvoluted XPS spectra of $Cu_1/CN$ and $Cu_1/CN/Al_2O_3$ in the Cu $2p_{3/2}$ region. (d) EPR spectra of $Cu_1/CN$ and $Cu_1/CN/Al_2O_3$. (e) N 1s XPS fitting analysis of $Cu_1/CN$ and $Cu_1/CN/Al_2O_3$. (f) DFT calculation studies on the oxidation state of SA Cu species in different coordination structures.

$Cu_1/CN/Al_2O_3$, which provides more proof of SA Cu species in them.[50–52] It is noteworthy that the oxidation states of the two SA Cu species are quite different from those of each other as indicated by their X-ray absorption near-edge structure (XANES) spectra (Fig. 2b). The adsorption peak ascribed to the dipole-allowed 1s → 4p transition of Cu is close to that of $Cu_2O$ for $Cu_1/CN$ (*ca.* 8982.5 eV) while it is closer to that of CuO for $Cu_1/CN/Al_2O_3$ (*ca.* 8986.1 eV) with differently intense white line peaks (*ca.* ~8996.0 eV), indicating the higher oxidation state of Cu species in $Cu_1/CN/Al_2O_3$. This conclusion can also be drawn from X-ray photoelectron spectroscopy (XPS) spectra in the Cu 2p region. The deconvoluted Cu $2p_{3/2}$ XPS peak indicates that $Cu_1/CN$ involves one major Cu species at a binding energy of 932.0 eV with the other minor Cu species at a binding energy of 934.3 eV. Meanwhile, for $Cu_1/CN/Al_2O_3$, a solely dominant peak at 933.0 eV can be deconvoluted from its Cu $2p_{3/2}$ XPS spectrum, illustrating the higher oxidation state of its Cu species compared to most Cu species in $Cu_1/CN$ (Fig. 2c). Moreover, electron paramagnetic resonance (EPR) studies found that $Cu_1/CN/Al_2O_3$ exhibits a notable Cu(ɪɪ) signal ($g = 2.045$), while $Cu_1/CN$ just displays a relatively weak Cu(ɪɪ) signal at a different $g$ value of 1.997 (Fig. 2d).[53–55] Given Cu(ɪ) species is silent in EPR, it is apparent that $Cu_1/CN$ contains a majority of Cu(ɪ) species and so leads to its lower oxidation state of Cu in contrast to $Cu_1/CN/Al_2O_3$ which contains predominant Cu(ɪɪ) species.[54]

The character of the CN carrier is next probed on the two catalysts. The CN carriers in $Cu_1/CN/Al_2O_3$ and $Cu_1/CN$ both display pyridinic-N (398.7 eV) as the major doped N species with minor amounts of pyrrolic-N (399.8 eV) and graphitic-N (400.9 eV), disclosed by deconvoluted N 1s XPS spectra (Fig. 2e, for fitting parameters see Table S1†).[54] However, the content of N species in the CN of $Cu_1/CN/Al_2O_3$ decreases a lot compared to that of $Cu_1/CN$ according to the significantly lower intensity of the pyridinic-N signal for $Cu_1/CN/Al_2O_3$ in soft X-ray absorption spectroscopy (sXAS) spectra (Fig. S8†). This result is also proved by elemental analyses which indicate that the content of N in $Cu_1/CN/Al_2O_3$ is just 1.04 wt% which is much less than that of $Cu_1/CN$ (30.77 wt%) (Table S2†). The more sparse N atoms result from the CN carrier being thin enough in $Cu_1/CN/Al_2O_3$ instead of the thick nanosheet morphology in $Cu_1/CN$. It should be noted that, owing to the decrease of N atoms, the ratio of N to Cu reduced a lot from 18.66 for $Cu_1/CN$ to 1.07 for $Cu_1/CN/Al_2O_3$ (Table S2†). It is predictable that fewer N atoms can lead to a smaller N coordination number for Cu centers in $Cu_1/CN/Al_2O_3$. This can be revealed by the EXAFS fitting analysis where the N coordination number of Cu is 3.2 for $Cu_1/CN$ while it is just 1.9 for $Cu_1/CN/Al_2O_3$ (Fig. S9†).

To confirm the lower-coordination structure, density functional theory (DFT) calculations are carried out to analyze the feature of SA Cu centers on the CN carrier with different coordination structures (Fig. S10 and Table S3†). Considering that N atoms in pure CN are abundant, Cu centers in $Cu_1/CN$ can exist as $Cu–N_3$ and $Cu–N_4$ structures as commonly reported in previous studies of CN supported SA Cu catalysts.[56–58] For increasing unsaturated coordination sites, the $Cu–N_2$ structure of Cu centers may be present in $Cu_1/CN/Al_2O_3$. Therefore, since the main N species in the CN of the two catalysts is pyridinic-N, the potential $Cu–N_4$, $Cu–N_3$ and $Cu–N_2$ structures with pyridinic-N coordination are simulated to explore their differences (Fig. 2f). It turns out that the charge of Cu in $Cu–N_2$

(0.712$e$) lies right between that in Cu–N$_3$ (0.668$e$) and Cu–N$_4$ (0.955$e$). This conclusion is consistent with the observation from Cu 2p$_{3/2}$ XPS spectra that the oxidation state of Cu in Cu$_1$/CN/Al$_2$O$_3$ is between that of the two Cu species in Cu$_1$/CN. This strongly verifies the lower coordinated Cu–N$_2$ structure in Cu$_1$/CN/Al$_2$O$_3$ instead of Cu–N$_3$ and Cu–N$_4$ structures in Cu$_1$/CN.

The performance of Cu$_1$/CN/Al$_2$O$_3$ and Cu$_1$/CN for transfer hydrogenation of alkynes is evaluated to clarify the influence of distinct coordination structures. Delightfully, the hydrogenation of phenylacetylene proceeds smoothly over Cu$_1$/CN/Al$_2$O$_3$ with AB as the hydrogen source (Fig. 3a). The product styrene is obtained in 94% yield and 99% selectivity without potential ethylbenzene by-product detected by gas chromatography-mass spectrometry (GC-MS) analysis (Fig. S11†). The turnover number (TON) is calculated to be 74 which is greater than that of reported heterogeneous non-noble metal based catalysts (Table S4†). Meanwhile, over Cu$_1$/CN, this hydrogenation reaction fails to occur under the same conditions. A pure Al$_2$O$_3$ supported SA Cu catalyst (Cu$_1$/Al$_2$O$_3$) is also prepared for comparison, and it possesses uniformly dispersed Cu species with a loading content of 0.5 wt% as revealed by STEM, EDX elemental mapping, XAS, and ICP-OES analyses (Fig. S12 and S13†). This Cu$_1$/Al$_2$O$_3$ exhibits a very poor activity in contrast to Cu$_1$/CN/Al$_2$O$_3$. Clean CN/Al$_2$O$_3$ is also inert for the reaction. Thus, it is concluded that the great performance of Cu$_1$/CN/Al$_2$O$_3$ derives from the distinct structure of the SA Cu species on CN from that of Cu$_1$/CN. A recycling test is conducted to evaluate the stability of Cu$_1$/CN/Al$_2$O$_3$. It shows that Cu$_1$/CN/Al$_2$O$_3$ can be reused at least five times without obvious loss of activity and selectivity at a relatively low conversion level (Fig. 3b). The loading content of Cu in the catalyst remains nearly the same as 0.97 wt% after the reaction as indicated by ICP-OES. STEM and EDX elemental mapping analyses manifest homogeneously dispersed Cu components and unchanged morphology in the recovered Cu$_1$/CN/Al$_2$O$_3$ (Fig. S14†). This demonstrates the good stability of Cu$_1$/CN/Al$_2$O$_3$ for such transfer hydrogenation reactions.

We next explore the impact of substrate categories on the catalytic performance of Cu$_1$/CN/Al$_2$O$_3$. As displayed in Fig. 4, phenylacetylene derivatives with electron-donating functional groups (MeO$^-$, $t$Bu$^-$, and Me$^-$) can be transformed into alkenes in good yields and selectivities (2b–2d), while those with electron-withdrawing functional groups (Br$^-$ and Cl$^-$) suffer from relatively low conversions (2e and 2f) for longer reaction time. This discloses that alkyne substrates have an electronic effect on the catalytic behavior of Cu$_1$/CN/Al$_2$O$_3$, where electron-poor alkynes can decrease the catalytic efficiency. The *meta*-methyl and *ortho*-methyl substituted phenylacetylenes are both hydrogenated into the corresponding alkenes (2h and 2i) with high conversions and selectivities, but the more steric naphthyl acetylene lowers the hydrogenation efficiency with just 83% conversion (2i), indicating the steric effect of substrates on the performance of Cu$_1$/CN/Al$_2$O$_3$. In addition, the hydrogenation of internal aryl alkynes like diphenylacetylene and 1-phenyl-1-propyne also proceeds over Cu$_1$/CN/Al$_2$O$_3$ with decreased conversions of 89% and 87% to provide alkene products with quantitative selectivities (2j and 2k). As for aliphatic alkynes such as cyclohexylacetylene, Cu$_1$/CN/Al$_2$O$_3$ exhibits an unchanged catalytic efficiency to convert it into the target cyclohexylethylene (2l) with 99% conversion and 98% selectivity.

The prominent performance of Cu$_1$/CN/Al$_2$O$_3$ with respect to Cu$_1$/CN can be attributed to the more unsaturated coordination of Cu centers caused by the Al$_2$O$_3$ compounding CN strategy. To
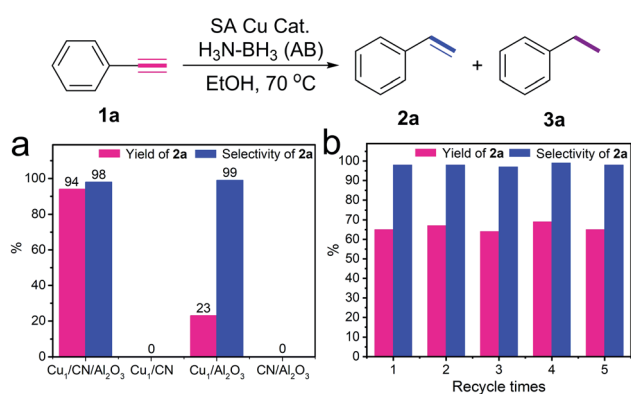


**Fig. 3** Performance evaluation for transfer hydrogenation of alkynes. (a) Activity evaluation of SA Cu catalysts for transfer hydrogenation of phenylacetylene. Standard reaction conditions: phenylacetylene (1a, 0.2 mmol), AB (1.0 mmol) in EtOH (4.0 mL) at 70 °C for 8 h with the catalyst: Cu$_1$/CN/Al$_2$O$_3$ (16.9 mg, Cu = 1.0 mol%), Cu$_1$/CN (9.8 mg, Cu = 1.0 mol%), Cu$_1$/Al$_2$O$_3$ (25.6 mg Cu = 1.0 mol%), CN/Al$_2$O$_3$ (16.9 mg). Yields are determined by gas chromatography (GC) analysis with dodecane as the internal standard. Selectivities are determined by GC-MS analysis. (b) Recycling test of Cu$_1$/CN/Al$_2$O$_3$ for transfer hydrogenation of phenylacetylene.
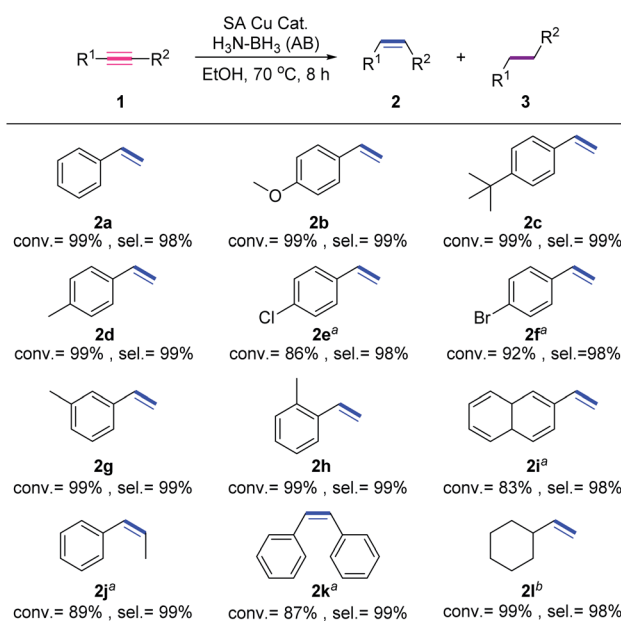


**Fig. 4** Substrate scope of transfer hydrogenation of alkynes over Cu$_1$/CN/Al$_2$O$_3$. Standard reaction conditions: substrate 1 (0.20 mmol), AB (1.0 mmol), Cu$_1$/CN/Al$_2$O$_3$ (16.9 mg, Cu = 1.0 mol%) in EtOH (4.0 mL) at 70 °C for 8 h. Conversion of 1 (conv.) is determined by GC analysis with dodecane as the internal standard. Selectivity of 2 (sel.) is determined by GC-MS analysis. [a]Reaction time is prolonged to 12 h. [b]Reaction time is shortened to 6 h.
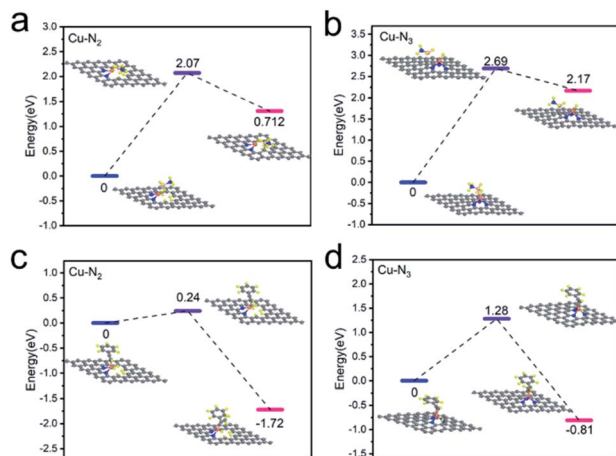
**Fig. 5** Investigations on the source of the improved activity. (a) DFT calculation studies on the hydrogen transfer from AB molecule to $Cu_1$/$CN$/$Al_2O_3$. (b) DFT calculation studies on the hydrogen transfer from AB molecule to $Cu_1$/$CN$. (c) DFT calculation studies on the transfer hydrogenation of phenylacetylene over $Cu_1$/$CN$/$Al_2O_3$. (d) DFT calculation studies on the transfer hydrogenation of phenylacetylene over $Cu_1$/$CN$.

gain more insight into the relationship between the performance and unsaturated coordination structures, DFT calculations are performed to analyze the transfer hydrogenation pathway over the two catalysts. Based on characterization results, the $Cu–N_2$ and $Cu–N_3$ models are constructed to simulate $Cu_1$/$CN$/$Al_2O_3$ and $Cu_1$/$CN$. The adsorption performance of AB molecules on the two SA Cu catalysts is firstly investigated for the reason that the initial step of the transfer hydrogenation is a hydrogen species shift from AB molecules to active Cu centers.[59,60] The energy barrier of this process is 2.07 eV on the $Cu–N_2$ structure and 2.69 eV higher on the $Cu–N_3$ structure, suggesting a more favorable hydrogen transfer on the former (Fig. 5a and b). Over hydrogenated $Cu–N_2$ and $Cu–N_3$ structures, the following transfer of hydrogen species to alkynes is next investigated. The phenylacetylene can adsorb on the hydrogenated Cu center in the $Cu–N_2$ structure, and the energy barrier of the hydrogen species shift to phenylacetylene is as low as 0.24 eV (Fig. 5c). Meanwhile, for the $Cu–N_3$ structure, since the hydrogenated Cu center is coordination-saturated, the adsorption of phenylacetylene is hindered. In order to achieve the hydrogenation process, a spillover hydrogenation procedure may be involved.[61] The hydrogen species shifts from the Cu center to the *ortho* carbon to provide the adsorption site for phenylacetylene (Fig. S15†), and then transfers back to realize the hydrogenation reaction (Fig. 5d). Even so, the total energy barrier of such procedures comes to 2.62 eV which is significantly higher than that of the hydrogenation process on the $Cu–N_2$ structure, demonstrating the dramatic difficulty in the transfer hydrogenation reaction.

## Conclusions

In summary, we report that reducing the coordination sites of a SA Cu catalyst on CN can achieve remarkable performance for

selective transfer hydrogenation of alkynes. Through compounding with $Al_2O_3$, the CN carrier becomes very thin with fewer N atoms, leading to a more unsaturated $Cu–N_2$ coordination structure of independent Cu centers. Unlike the pure CN supported SA Cu catalyst with common $Cu–N_3$ and $Cu–N_4$ structures disabling the transfer hydrogenation of alkynes, the SA Cu catalyst anchored by decreased N atoms exhibits great activity for the hydrogenation reaction, furnishing various alkenes with good activity and selectivity. The decrease of coordinated N atoms makes SA Cu sites superior for abstracting hydrogen from ammonia–borane and adsorbing alkyne substrates to reach the transfer hydrogenation process, which causes the outstanding catalytic behavior of the catalyst. This work confirms that increasing the unsaturated coordination sites of SA catalysts *via* precise regulation of their coordination environment can readily and efficiently change the catalytic performance, providing new opportunities to develop better-performing SA catalysts for heterogeneous catalysis.

## Data availability

Data associated with this article, including synthesis, characterization, and experimental procedures, are available in the ESI.†

## Author contributions

X. Z. performed the experiments, collected and analyzed the data, and wrote the paper. H. L. conducted the density functional theory calculation and analysis. Y. Q., Z. Z., Q. X. and G. M. assisted in HR-TEM, STEM, XAS and EDX elemental mapping characterizations. W. Y. helped with the sXAS analysis. L. G. assisted in the AC HAADF-STEM characterization. J. Z., D. W. and Y. L. conceived the experiments, planned the synthesis, analyzed the results, and wrote the paper.

## Conflicts of interest

There are no conflicts to declare.

## Acknowledgements

## Notes and references

1 A. Wang, J. Li and T. Zhang, *Nat. Rev. Chem.*, 2018, **2**, 65–81.

2 X. Cui, W. Li, P. Ryabchuk, K. Junge and M. Beller, *Nat. Catal.*, 2018, **1**, 385–397.

3 J. Yang, W. Li, S. Tan, K. Xu, Y. Wang, D. Wang and Y. Li, *Angew. Chem., Int. Ed.*, 2021, **60**, 19085–19091.

4 J. Yang, W. Li, D. Wang and Y. Li, *Small Struct.*, 2021, **2**, 20051.

5 Y. Zhang, L. Guo, L. Tao, Y. Lu and S. Wang, *Small Methods*, 2019, **3**, 1800406.

6 L. Fan, P. F. Liu, X. Yan, L. Gu, Z. Z. Yang, H. G. Yang, S. Qiu and X. Yao, *Nat. Commun.*, 2016, **7**, 10667.

7 Z.-Y. Wu, M. Karamad, X. Yong, Q. Huang, D. A. Cullen, P. Zhu, C. Xia, Q. Xiao, M. Shakouri, F.-Y. Chen, J. Y. Kim, Y. Xia, K. Heck, Y. Hu, M. S. Wong, Q. Li, I. Gates, S. Siahrostami and H. Wang, *Nat. Commun.*, 2021, **12**, 2870.

8 Q. Qu, S. Ji, Y. Chen, D. Wang and Y. Li, *Chem. Sci.*, 2021, **12**, 4201–4215.

9 L. Wang, E. Guan, J. Zhang, J. Yang, Y. Zhu, Y. Han, M. Yang, C. Cen, G. Fu, B. C. Gates and F.-S. Xiao, *Nat. Commun.*, 2018, **9**, 1362.

10 J. Zhang, Z. Wang, W. Chen, Y. Xiong, W.-C. Cheong, L. Zheng, W. Yan, L. Gu, C. Chen, Q. Peng, P. Hu, D. Wang and Y. Li, *Chem*, 2020, **6**, 725–737.

11 Z. Chen, E. Vorobyeva, S. Mitchell, E. Fako, M. A. Ortuño, N. López, S. M. Collins, P. A. Midgley, S. Richard, G. Vilé and J. Pérez-Ramírez, *Nat. Nanotechnol.*, 2018, **13**, 702–707.

12 Y. Xiong, W. Sun, Y. Han, P. Xin, X. Zheng, W. Yan, J. Dong, J. Zhang, D. Wang and Y. Li, *Nano Res.*, 2021, **14**, 2418–2423.

13 X. Li, X. Huang, S. Xi, S. Miao, J. Ding, W. Cai, S. Liu, X. Yang, H. Yang, J. Gao, J. Wang, Y. Huang, T. Zhang and B. Liu, *J. Am. Chem. Soc.*, 2018, **140**, 12469–12475.

14 G. Meng, K. Ji, W. Zhang, Y. Kang, Y. Wang, P. Zhang, Y. G. Wang, J. Li, T. Cui, X. Sun, T. Tan, D. Wang and Y. Li, *Chem. Sci.*, 2021, **12**, 4139–4146.

15 S. Bai, F. Liu, B. Huang, F. Li, H. Lin, T. Wu, M. Sun, J. Wu, Q. Shao, Y. Xu and X. Huang, *Nat. Commun.*, 2020, **11**, 954.

16 X. Liu, Y. Jiao, Y. Zheng, M. Jaroniec and S. Z. Qiao, *J. Am. Chem. Soc.*, 2019, **141**, 9664–9672.

17 T. Zhang, X. Nie, W. Yu, X. Guo, C. Song, R. Si, Y. Liu and Z. Zhao, *iScience*, 2019, **22**, 97–108.

18 W. Liu, L. Zhang, X. Liu, X. Liu, X. Yang, S. Miao, W. Wang, A. Wang and T. Zhang, *J. Am. Chem. Soc.*, 2017, **139**, 10790–10798.

19 L. Han, S. Song, M. Liu, S. Yao, Z. Liang, H. Cheng, Z. Ren, W. Liu, R. Lin, G. Qi, X. Liu, Q. Wu, J. Luo and H. L. Xin, *J. Am. Chem. Soc.*, 2020, **142**, 12563–12567.

20 Y. Pan, R. Lin, Y. Chen, S. Liu, W. Zhu, X. Cao, W. Chen, K. Wu, W.-C. Cheong, Y. Wang, L. Zheng, J. Luo, Y. Lin, Y. Liu, C. Liu, J. Li, Q. Lu, X. Chen, D. Wang, Q. Peng, C. Chen and Y. Li, *J. Am. Chem. Soc.*, 2018, **140**, 4218–4221.

21 X. Hu, G. Luo, Q. Zhao, D. Wu, T. Yang, J. Wen, R. Wang, C. Xu and N. Hu, *J. Am. Chem. Soc.*, 2020, **142**, 16776–16786.

22 J. Li, L. Jiao, E. Wegener, L. L. Richard, E. Liu, A. Zitolo, M. T. Sougrati, S. Mukerjee, Z. Zhao, Y. Huang, F. Yang, S. Zhong, H. Xu, A. J. Kropf, F. Jaouen, D. J. Myers and Q. Jia, *J. Am. Chem. Soc.*, 2020, **142**, 1417–1423.

23 L. Zhang, A. Wang, W. Wang, Y. Huang, X. Liu, S. Miao, J. Liu and T. Zhang, *ACS Catal.*, 2015, **5**, 6563–6572.

24 S. Chen, Y. Li, Z. Bu, F. Yang, J. Luo, Q. An, Z. Zeng, J. Wang and S. Deng, *J. Mater. Chem. A*, 2021, **9**, 1705–1712.

25 D. Deng, X. Chen, L. Yu, X. Wu, Q. Liu, Y. Liu, H. Yang, H. Tian, Y. Hu, P. Du, R. Si, J. Wang, X. Cui, H. Li, J. Xiao, T. Xu, J. Deng, F. Yang, P. N. Duchesne, P. Zhang, J. Zhou, L. Sun, J. Li, X. Pan and X. Bao, *Sci. Adv.*, 2015, **1**, e1500462.

26 H. Wu, H. Li, X. Zhao, Q. Liu, J. Wang, J. Xiao, S. Xie, R. Si, F. Yang, S. Miao, X. Guo, G. Wang and X. Bao, *Energy Environ. Sci.*, 2016, **9**, 3736–3745.

27 Y. Chen, R. Gao, S. Ji, J. Li, K. Tang, P. Jiang, H. Hu, Z. Zhang, H. Hao, Q. Qu, X. Liang, W. Chen, J. Dong, D. Wang and Y. Li, *Angew. Chem., Int. Ed.*, 2021, **60**, 3212–3221.

28 Y. Pan, Y. Chen, K. Wu, Z. Chen, S. Liu, X. Cao, W.-C. Cheong, T. Meng, J. Luo, L. Zheng, C. Liu, D. Wang, Q. Peng, J. Li and C. Chen, *Nat. Commun.*, 2019, **10**, 4290.

29 Z. Geng, Y. Cao, W. Chen, X. Kong, Y. Liu, T. Yao and Y. Lin, *Appl. Catal., B*, 2019, **240**, 234–240.

30 T. Sun, S. Mitchell, J. Li, P. Lyu, X. Wu, J. Perez-Ramirez and J. Lu, *Adv. Mater.*, 2021, **33**, e2003075.

31 H. Zhang, J. Li, S. Xi, Y. Du, X. Hai, J. Wang, H. Xu, G. Wu, J. Zhang, J. Lu and J. Wang, *Angew. Chem., Int. Ed.*, 2019, **58**, 14871–14876.

32 Y. Zhang, L. Jiao, W. Yang, C. Xie and H.-L. Jiang, *Angew. Chem., Int. Ed.*, 2021, **60**, 7607–7611.

33 Y. Wang, G. Jia, X. Cui, X. Zhao, Q. Zhang, L. Gu, L. Zheng, L. H. Li, Q. Wu, D. J. Singh, D. Matsumura, T. Tsuji, Y.-T. Cui, J. Zhao and W. Zheng, *Chem*, 2021, **7**, 436–449.

34 X. Wang, Z. Chen, X. Zhao, T. Yao, W. Chen, R. You, C. Zhao, G. Wu, J. Wang, W. Huang, J. Yang, X. Hong, S. Wei, Y. Wu and Y. Li, *Angew. Chem., Int. Ed.*, 2018, **57**, 1944–1948.

35 A. Henrick, *Tetrahedron*, 1977, **33**, 1845–1889.

36 G. C. Tron, T. Pirali, G. Sorba, F. Pagliai, S. Busacca and A. A. Genazzani, *J. Med. Chem.*, 2006, **49**, 3033–3044.

37 T. Brown, H. Holt Jr and M. Lee, in *Heterocyclic Antitumor Antibiotics*, ed. M. Lee, Springer Berlin Heidelberg, Berlin, Heidelberg, 2006, pp. 1–51, DOI: DOI: 10.1007/7081_003.

38 G. M. Richardson, I. Douair, S. A. Cameron, J. Bracegirdle, R. A. Keyzers, M. S. Hill, L. Maron and M. D. Anker, *Nat. Commun.*, 2021, **12**, 3147.

39 X. Lu, B. Xiao, Z. Zhang, T. Gong, W. Su, J. Yi, Y. Fu and L. Liu, *Nat. Commun.*, 2016, **7**, 11129.

40 K. Dong, X. Fang, S. Gülak, R. Franke, A. Spannenberg, H. Neumann, R. Jackstell and M. Beller, *Nat. Commun.*, 2017, **8**, 14117.

41 T. Mitsudome, M. Yamamoto, Z. Maeno, T. Mizugaki, K. Jitsukawa and K. Kaneda, *J. Am. Chem. Soc.*, 2015, **137**, 13452–13455.

42 S. P. Desai, J. Ye, J. Zheng, M. S. Ferrandon, T. E. Webber, A. E. Platero-Prats, J. Duan, P. Garcia-Holley, D. M. Camaioni, K. W. Chapman, M. Delferro, O. K. Farha, J. L. Fulton, L. Gagliardi, J. A. Lercher, R. L. Penn, A. Stein and C. C. Lu, *J. Am. Chem. Soc.*, 2018, **140**, 15309–15318.

43 S. Wang, Z. Xin, X. Huang, W. Yu, S. Niu and L. Shao, *Phys. Chem. Chem. Phys.*, 2017, **19**, 6164–6168.

44 R. Guo, Q. Chen, X. Li, Y. Liu, C. Wang, W. Bi, C. Zhao, y. Guo and M. Jin, *J. Mater. Chem. A*, 2019, **7**, 4714–4720.

45 J. Hori, K. Murata, T. Sugai, H. Shinohara, R. Noyori, N. Arai, N. Kurono and T. Ohkuma, *Adv. Synth. Catal.*, 2009, **351**, 3143–3149.

46 X. Wen, X. Shi, X. Qiao, Z. Wu and G. Bai, *Chem. Commun.*, 2017, **53**, 5372–5375.

47 V. Polshettiwar, B. Baruwati and R. S. Varma, *Green Chem.*, 2009, **11**, 127–131.

48 S. Fu, N. Y. Chen, X. Liu, Z. Shao, S. P. Luo and Q. Liu, *J. Am. Chem. Soc.*, 2016, **138**, 8588–8594.

49 S. Mou, Y. Lu and Y. Jiang, *Appl. Surf. Sci.*, 2016, **384**, 258–262.

50 M. Abdel-Mageed, B. Rungtaweevoranit, M. Parlinska-Wojtan, X. Pei, O. M. Yaghi and R. J. Behm, *J. Am. Chem. Soc.*, 2019, **141**, 5201–5210.

51 F. Li, G.-F. Han, H.-J. Noh, S.-J. Kim, Y. Lu, H. Y. Jeong, Z. Fu and J.-B. Baek, *Energy Environ. Sci.*, 2018, **11**, 2263–2269.

52 P. Ren, Q. Li, T. Song and Y. Yang, *ACS Appl. Mat. Interfaces*, 2020, **12**, 27210–27218.

53 E. Crusson-Blouet, A. Aboukais, C. F. Aissi and M. Guelton, *Chem. Mater.*, 1992, **4**, 1129–1131.

54 T. Zhang, D. Zhang, X. Han, T. Dong, X. Guo, C. Song, R. Si, W. Liu, Y. Liu and Z. Zhao, *J. Am. Chem. Soc.*, 2018, **140**, 16936–16940.

55 R. Kydd, W. Y. Teoh, K. Wong, Y. Wang, J. Scott, Q.-H. Zeng, A.-B. Yu, J. Zou and R. Amal, *Adv. Funct. Mater.*, 2009, **19**, 369–377.

56 M. Tong, F. Sun, Y. Xie, Y. Wang, Y. Yang, C. Tian, L. Wang and H. Fu, *Angew. Chem., Int. Ed.*, 2021, **60**, 14005–14012.

57 C. Huang, L. Zheng, W. Feng, A. Guo, X. Gao, Z. Long and X. Qiu, *ACS Sustainable Chem. Eng.*, 2020, **8**, 14030–14038.

58 X. Lu, S. Gao, H. Lin, L. Yu, Y. Han, P. Zhu, W. Bao, H. Yao, Y. Chen and J. Shi, *Adv. Mater.*, 2020, **32**, 2002246.

59 G. Jaiswal, V. G. Landge, M. Subaramanian, R. G. Kadam, R. Zbořil, M. B. Gawande and E. Balaraman, *ACS Sustainable Chem. Eng.*, 2020, **8**, 11058–11068.

60 V. R. Bakuru, D. Samanta, T. K. Maji and S. B. Kalidindi, *Dalton Trans.*, 2020, **49**, 5024–5028.

61 R. Prins, *Chem. Rev.*, 2012, **112**, 2714–2738.